A Spin System Model for Coupled-Cavity Masers

J. Shell[1]

The software for designing coupled-cavity masers has been extended to include the effects of the ruby spin system. Two computer programs based on the mode-matching algorithm are used. The first program calculates the magnetic susceptibility in the ruby-filled cavity. The second program uses this information to calculate the scattering parameters. The effects of the ruby spin system are modeled in both the absorptive and emissive states. Several examples of the model are presented.

I. Introduction

The ruby spin system is the collection of weakly interacting magnetic dipole moments associated with the chromium ions in the aluminum oxide crystal lattice. Macroscopically, they appear as a weak paramagnetic system. The population inversion achieved with the states of these dipoles in an external magnetic field is responsible for the amplification process in a maser. The recent 31.8- to 32.3-GHz (Ka-band) coupled-cavity maser design was done with a rectangular-waveguide mode-matching program developed by JPL [1]. The maser was designed with no explicit reference to the ruby spin system [2]. A better understanding of the maser and more accurate designs require that the effects of the spin system be included.

The earlier version of the mode-matching program characterizes the dielectric media by a complex relative dielectric constant, but otherwise includes no losses. The original Ka-band coupled-cavity maser design used the complex relative dielectric constant to create a loss in the cavity containing the ruby crystal. This loss can be thought of as representing a spin system with infinite line width and no reactance. However, the quantum transitions of the ruby spin system behave as resonant circuits. They have both a finite line width and reactive behavior. In addition, these components are temperature dependent. Furthermore, when the spin system is inverted, by pumping the ruby, the resistive and the reactive components change sign. This article presents a model useful for designing coupled-cavity masers that includes these effects.

An advantage of the model is its ability to predict the strength of the paramagnetic resonance. The strength of the spin resonance at a particular frequency is determined mainly by two factors. One factor is the polarization, direction, and strength of the rf magnetic field relative to the spin vector of the quantum transition. The rf magnetic field is determined by the geometry of the coupled cavities. The spin vector is determined by the strength and relative orientation of the external static magnetic field to the ruby c-axis. A second factor is the difference in spin population between the levels for which the transition

[1] Communications Ground Systems Section.

The research described in this publication was carried out by the Jet Propulsion Laboratory, California Institute of Technology, under a contract with the National Aeronautics and Space Administration.

occurs. The physical temperature of the ruby and the spacing of the four ground state levels determine this difference. The number of spins available for a transition at a given frequency is also dependent on the static magnetic field distribution. The static magnetic field may not be uniform, but shaped in such a way as to broaden the ruby line width and increase the bandwidth of the amplifier. The model attempts to include all of these effects.

By changing the physical temperature in the model, one can determine when the spin system becomes critically coupled, or matched, to the generator equivalent resistance. The reflected power on resonance, if the ruby is absorbing, will be essentially equal to zero. Such a spin system, when pumped (inverted), will oscillate. An even stronger spin resonance will result in less complete power absorption. This often is referred to as an under-coupled system. The radio frequency energy added to the cavity by the spin system when pumped exceeds the cavity losses due to external loading and dissipation in the walls and dielectric. Such a system most likely will oscillate. A weaker spin resonance than the critically coupled case also results in less than complete power absorption. This is referred to as an over-coupled system. The radio frequency energy added to the cavity by the spin system when pumped does not exceed all the losses mentioned above. Such a system can have a stable gain when pumped.

The approach used is to generalize the scattering-parameter mode-matching program to include a frequency- and position-dependent complex magnetic permeability. The frequency- and position-dependent portion of the permeability is provided by a complex magnetic susceptibility. Another program, also based on the mode-matching algorithm, is used to calculate the position-dependent portion of the susceptibility.

The model evaluates the rf magnetic field in the ruby cavity in order to reduce the susceptibility tensor to a complex scalar quantity. The rf magnetic field is calculated using an improved version of a computer Fortran program described previously [3]. The expression for the susceptibility tensor and its reduction to a scalar is addressed in Section II. Since we are interested in the maser as an amplifier, particular attention was given to the problem of inverting the ruby to predict the gain. This involves understanding the characteristics of the propagation constant above and below cutoff for a waveguide filled with active material. This is addressed in Section III. Some of the limitations of the model are discussed in Section IV, and several examples are presented in Section V.

II. Magnetic Susceptibility of Ruby

The magnetic susceptibility of single crystal ruby is anisotropic and is described by a rather remarkable equation [4,5]. It is given by

$$\overline{\overline{\chi}} = \frac{\pi\mu_o}{h}(g_s\beta)^2(n_i - n_j)\{h(f - f_o) - jg(f - f_o)\}\overline{\overline{S}} \tag{1}$$

Here h, μ_o, g_s, and β are Planck's constant, the permeability of free space, the spectroscopic splitting factor, and the Bohr magneton, respectively. Also, $(n_i - n_j)$ is the difference in the number of spins per unit volume in states i and j. The line-shape functions describe the variation of the susceptibility away from the resonant frequency, f_o. Two line-shape functions are used. They are denoted by $g(f - f_o)$ and $h(f - f_o)$, respectively. The line-shape functions are given by

$$h(f) = \frac{4(f_o - f)}{\pi(\Delta f_L)^2 + 4\pi(f - f_o)^2} \tag{2}$$

$$g(f) = \frac{2\Delta f_L}{\pi(\Delta f_L)^2 + 4\pi(f - f_o)^2} \tag{3}$$

A plot of these functions is shown in Fig. 1 for $f_0 = 31.5$ and $\Delta f_L = 0.060$. They are related by a Kramer–Kronig relationship. The matrix $\overline{\overline{S}} = \overrightarrow{S}\,\overrightarrow{S^*}$, where $\overrightarrow{S}$ is the quantum mechanical spin vector operator. Normally $\overrightarrow{S}$ appears sandwiched between quantum states of the ruby. That is,

$$\langle i|\,\overrightarrow{S}\,|j\rangle = \langle i|\,S_x\,\overrightarrow{x} + S_y\,\overrightarrow{y} + S_z\,\overrightarrow{z}\,|j\rangle = \langle i|\,S_x\,|j\rangle\,\overrightarrow{x} + \langle i|\,S_y\,|j\rangle\,\overrightarrow{y} + \langle i|\,S_z\,|j\rangle\,\overrightarrow{z} \tag{4}$$

The evaluation of this quantity is discussed in detail in [6]. It is different for each quantum transition. It is important in what follows to note that the matrix $\overline{\overline{S}}$ is hermitian. (Notice that the x-, y-, z-directions in [6] correspond to the −x-, z-, y-directions in [3], respectively).

In general, the elements of the matrix $\overline{\overline{S}}$ are complex. This would appear to cause a mixture of $h(f)$ and $g(f)$ to be associated with the real and imaginary parts of $\overline{\overline{S}}$ for each element of $\overline{\overline{\chi}}$. However, if the susceptibility tensor is defined as

$$\overline{\overline{\chi}} = \overline{\overline{\chi'}} - j\overline{\overline{\chi''}} \tag{5}$$

and $\overline{\overline{\chi'}}$ and $\overline{\overline{\chi''}}$ are given by (as discussed by Siegman [4])

$$\overline{\overline{\chi'}} = \frac{1}{2}(\overline{\overline{\chi}} + \overline{\overline{\chi^\dagger}}) \tag{6a}$$

and

$$\overline{\overline{\chi''}} = \frac{j}{2}(\overline{\overline{\chi}} - \overline{\overline{\chi^\dagger}}) \tag{6b}$$

then everything works out. (The superscript "†" denotes the hermitian conjugate.) In the case of ruby, this reduces to

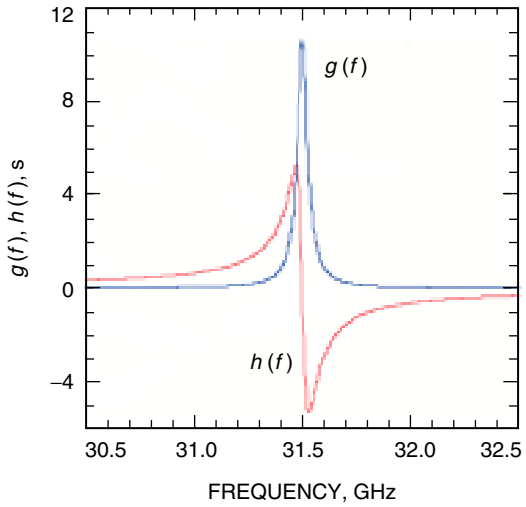

Fig. 1. The line-shape functions $g(f)$ and $h(f)$ for f_o = 31.5 GHz and Δf_L = 0.060.GHz.

$$\overline{\overline{\chi'}} = \frac{\pi\mu_o}{h}(g_s\beta)^2(n_i - n_j)h(f - f_o)\overline{\overline{S}} \tag{7}$$

$$\overline{\overline{\chi''}} = \frac{\pi\mu_o}{h}(g_s\beta)^2(n_i - n_j)g(f - f_o)\overline{\overline{S}} \tag{8}$$

As a result, $\overline{\overline{\chi'}}$ and $\overline{\overline{\chi''}}$ are also hermitian, and the real and imaginary parts of the susceptibility tensor are related by a Kramer–Kronig relationship.

Up to this point, everything has been kept rather general. However, to proceed further treating the susceptibility as a tensor quantity would be very complicated. If the tensor susceptibility could be replaced by an effective scalar susceptibility, then the analysis would be much simpler. The magnetic loading would be incorporated by changes to the waveguide propagation constant and the impedance of the waveguide modes. This is the approach used.

The derivation of the effective susceptibility is not long, but we leave a discussion of it to the Appendix. Here we only state the result. An effective scalar susceptibility is given by an expression of the form

$$\chi = \frac{\iint[\overrightarrow{H_o^*} \cdot \overline{\overline{\chi}} \cdot \overrightarrow{H_o}]ds}{\iint[\overrightarrow{H_o^*} \cdot \overrightarrow{H}_o]ds} \tag{9}$$

with dissipative and dispersive parts, respectively, given by

$$\chi'' = \frac{\iint[\overrightarrow{H_o^*} \cdot \overline{\overline{\chi''}} \cdot \overrightarrow{H_o}]ds}{\iint[\overrightarrow{H_o^*} \cdot \overrightarrow{H}_o]ds} \tag{10a}$$

and

$$\chi' = \frac{\iint[\overrightarrow{H_o^*} \cdot \overline{\overline{\chi'}} \cdot \overrightarrow{H_o}]ds}{\iint[\overrightarrow{H_o^*} \cdot \overrightarrow{H_o}]ds} \tag{10b}$$

Since the geometrical part of the susceptibility tensor is contained within the spin tensor, we are effectively defining an effective spin scalar. Thus, for both the dispersive and absorptive parts of the susceptibility, it is useful to define an effective spin scalar by

$$S = \frac{\iint[\overrightarrow{H_{rf}^*} \cdot \overline{\overline{S}} \cdot \overrightarrow{H_{rf}}]ds}{\iint[\overrightarrow{H_{rf}^*} \cdot \overrightarrow{H_{rf}}]ds} \tag{11}$$

In order to incorporate this into the mode-matching program, we define an effective spin scalar for planes normal to the direction of propagation (the z-direction). In particular, the effective spin as a function of the distance along the direction of propagation (the z-direction) in the ruby-filled cavity is given by

$$S_{eff}(z) = \frac{\iint_{\text{slice}} \overrightarrow{H_{rf}^*}(f, \overrightarrow{r}) \cdot (\overline{\overline{S}}) \cdot \overrightarrow{H_{rf}}(f, \overrightarrow{r})dxdy}{\iint_{\text{slice}} \overrightarrow{H_{rf}^*}(f, \overrightarrow{r}) \cdot \overrightarrow{H_{rf}}(f, \overrightarrow{r})dxdy} \tag{12}$$

where $\overrightarrow{r} = (x, y, z)$. (In the current version of the program, the fields are uniform in the y-direction, so the integration is only over the x-coordinate.) We approximate the integral by a summation. Then the spin scalar can be written (dropping the subscript "rf") as

$$S_{eff}(z) = \frac{\sum_{x_i} \overrightarrow{H^*}(f, \overrightarrow{r}) \cdot (\overline{\overline{S}}) \cdot \overrightarrow{H}(f, \overrightarrow{r})}{\sum_{x_i} \overrightarrow{H^*}(f, \overrightarrow{r}) \cdot \overrightarrow{H}(f, \overrightarrow{r})} \tag{13}$$

$\overrightarrow{H}(\overrightarrow{r})$ is the radio frequency magnetic field at location (x, y) and z appropriate to the slice of the ruby under consideration.

In summary, we can model the ruby spin system by including in our definition of the magnetic permeability a complex scalar susceptibility whose components are given by

$$\begin{pmatrix} \chi'_{eff}(f, z) \\ \chi''_{eff}(f, z) \end{pmatrix} = \frac{\pi \mu_o}{h} (g_s \beta)^2 (n_i - n_j) S_{eff}(z) \begin{pmatrix} h(f) \\ g(f) \end{pmatrix} \tag{14}$$

The procedure for modeling the ruby spin response involves two computer programs, both based on the mode-matching algorithm. In the first program, the ruby cavity in the maser structure is subdivided into a number of slices. The magnetic field is evaluated in the ruby cavity at a frequency near the center of the amplification band, and $S_{eff}(z)$ is calculated for each slice. Then the quantity given by

$$\chi_p(z) = \frac{\pi \mu_o}{h} (g_s \beta)^2 (n_i - n_j) S_{eff}(z) \tag{15}$$

is evaluated for each slice of the ruby. The first program creates an input data file suitable for use by the second program.

The second program uses the $\chi_p(z)$ calculated by the first program plus the line-shape functions $g(f)$ and $h(f)$ and calculates $\chi'_{eff}(z)$ and $\chi''_{eff}(z)$. Then a frequency- and position-dependent permeability is defined. The scattering parameters are calculated as in [1]. However, because the ruby can exhibit gain, the procedure for calculating the propagation constant has to be modified. This modification to the original scattering-parameter mode-matching program is discussed in the next section.

III. Waveguide Propagation Constant with Active or Lossy Material

The ruby used in masers is a weak paramagnetic material. The ac magnetic susceptibility is usually much less than one, so the deviation of the permeability tensor from unity is small. Although the deviation is small, it accounts for all the interesting effects mentioned in the introduction. The frequency-dependent scalar magnetic susceptibility derived in the previous section is used to calculate a complex permeability given by

$$\mu = \mu_o \left[1 + \chi'_{eff} - j\chi''_{eff}\right] \tag{16}$$

The complex permeability and complex permittivity are used to calculate the square of the propagation constant according to

$$\gamma^2 = k_c^2 - k^2 = k_c^2 - \omega^2 \mu \varepsilon \tag{17}$$

Here, k^2 is the square of the wave number of the medium filling the waveguide, and k_c^2 is the square of the cutoff wave number of the waveguide.

For the case where μ and ε have no imaginary components, γ^2 moves from right to left along the real axis of the complex plane as the frequency is increased, as shown in Fig. 2(a). Below the cutoff frequency of the waveguide, γ^2 is real and positive, and above the cutoff frequency, γ^2 is real and negative. The origin corresponds to the point where the propagation changes from being below cutoff to being above cutoff. If the system has a frequency-independent loss, then γ^2 moves from the right to the left on a line above the horizontal axis. The greater the loss, the further the line is above the horizontal axis. The location of the no-loss cutoff frequency is on the positive imaginary axis. A similar situation holds for the case of gain. Now γ^2 moves from the right to the left on a line below the horizontal axis. The greater the gain, the further the line is below the horizontal axis. Again, the frequency that corresponds to the origin in the lossless case corresponds to the point where the curve representing gain crosses the negative imaginary axis.

During the execution of the program, it is necessary to calculate $\gamma = \alpha + j\beta$. The calculation of the square root of γ^2 is not always obvious. If we think of γ^2 as a complex number in a polar representation, $re^{i\vartheta}$, then the square root is given by $\gamma = \sqrt{r}e^{i\vartheta/2}$. If γ^2 occupies the equivalent of two quadrants in the complex plane, we expect γ to occupy the equivalent of one quadrant of area of the complex plane.

This region corresponding to one quadrant can be divided further into two regions, corresponding to frequencies above the no-loss cutoff frequency and below the no-loss cutoff frequency. Furthermore, we expect the area of these two regions to be one-half of one quadrant of the complex plane.

We consider first the case of loss. The locus of points corresponding to the no-loss cutoff is the positive imaginary axis in the complex γ^2 plane. The phase angle of this ray is either +90 deg or −270 deg. Therefore, we expect this line in the complex γ plane to be either +45 deg or −135 deg. So we expect region B in Fig. 2(a) to map into either region B' or B'' in Fig. 2(b). But region B'' corresponds to gain, because α is negative there. So, B must map into B'. The same argument applies to region A in Fig. 2(a). It can map into either A' or A'' in Fig. 2(b). But, region A'' corresponds to gain, so it must map into region A'.

Now consider the case of gain. The locus of points corresponding to the no-loss cutoff frequency is the negative imaginary axis. The phase angle of this ray can be thought of as −90 deg or +270 deg. Therefore, we expect this line in the complex γ plane to be either +135 deg or −45 deg. So, we expect region C in Fig. 2(a) to map into either C' or C'' in Fig. 2(b). But, since region C corresponds to above cutoff with gain, we expect α to be negative in the corresponding region in the γ plane. Therefore, C must map into the region C'. Finally, we consider region D, the below-cutoff region with gain. It can map into either region D' or D'' in Fig. 2(b). We suggest that it map into the region D'. Consider the point Q in Fig. 2(a). It corresponds to a situation where there is very small gain (close to the real axis) and well below cutoff (far to the right). It will map into either the point Q' or the point Q'' in Fig. 2(b). Point Q' corresponds to a situation of loss, α is positive. Point Q'' corresponds to a situation of large gain, α is negative. Physically, point Q' makes more sense. Our final picture of the complex γ plane looks like Fig. 2(c). A Fortran routine was written to take the complex square root of γ^2. The routine examines the argument of γ^2. Depending on its location in Fig. 2(a), it is mapped into the correct part of the γ half-plane in Fig. 2(c).

In summary, Eq. (14) gives the real and imaginary parts of an effective scalar susceptibility for a particular quantum transition in ruby. It is specified once the temperature of the ruby, the magnitude and orientation of the external static magnetic field, and the rf magnetic field vector are specified. These

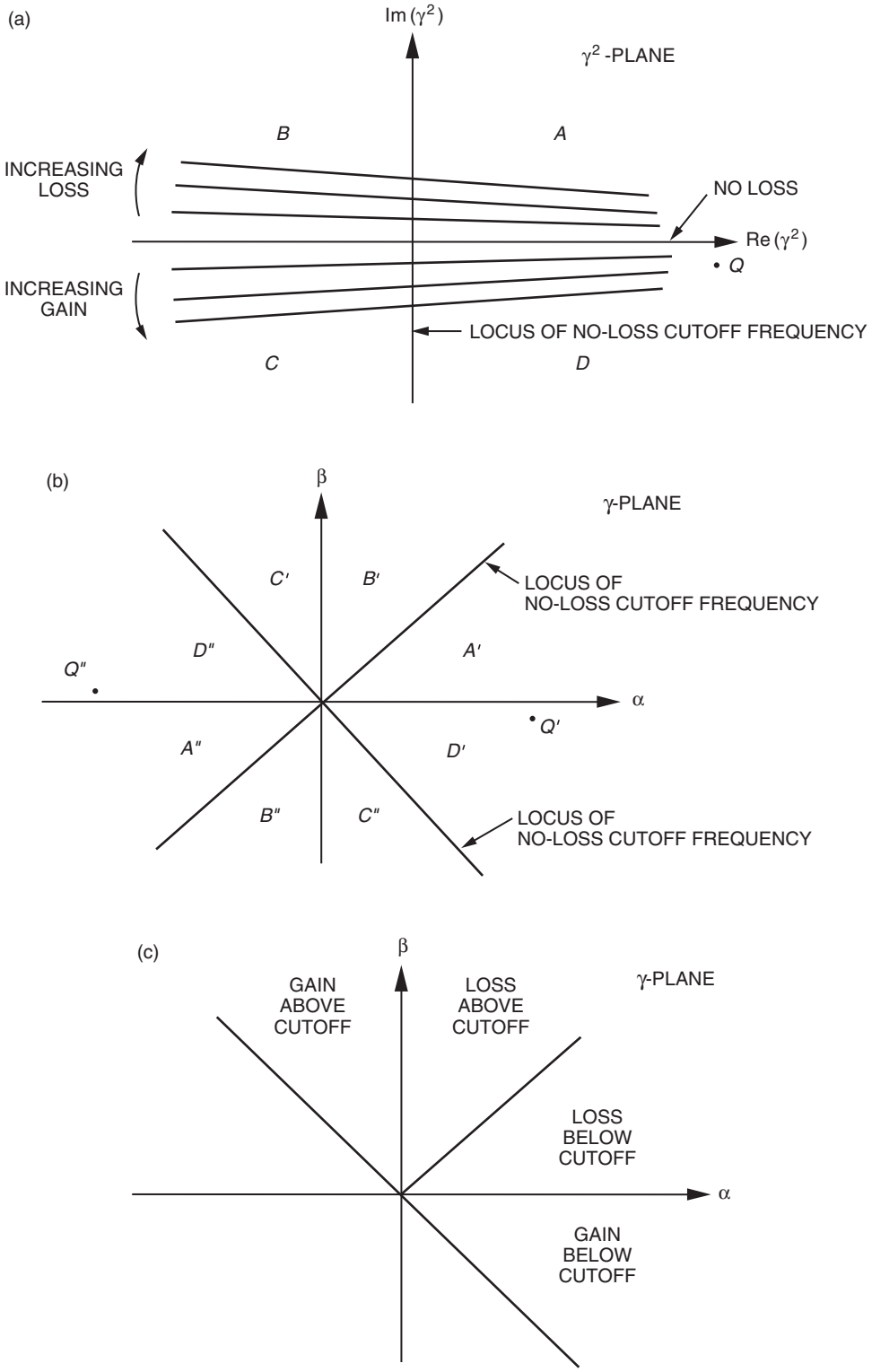

Fig. 2. Figures used to determine γ from knowledge of γ^2: (a) the behavior of γ^2 for systems with gain or loss above and below the waveguide cutoff frequency, (b) a general partition of the γ-plane based on the four quadrants in Fig. 2(a), and (c) the proper assignment of the partition in Fig. 2(b).

are used to calculate a complex magnetic permeability according to Eq. (16). The complex permeability, permittivity, and waveguide dimensions enable the calculation of γ^2 according to Eq. (17). Then the appropriate square root is taken as described above. The value of γ determined in this way replaces the previous value everywhere that it appears, including the waveguide mode impedances given by $Z_{TE} = (j\omega\mu/\gamma)$ and $Z_{TM} = (\gamma/j\omega\varepsilon)$.

IV. Assumptions and Limitations

The reason for developing the model is to predict and help understand the major factors influencing the maser performance. This model is intended to get the design close enough that a small amount of experimental adjustment will produce the desired product. It is not the intention of the model to include all possible effects. Nevertheless, some discussion of the various approximations and assumptions seems appropriate.

We assume the change in the electromagnetic field shape and magnitude inside the cavity per unit distance due to the presence of the spin system is small. This approximation was used when the perturbed fields were replaced by the unperturbed fields in Eq. (A-1). This means the predictions of the program will be better for low-gain cavities.

We do not include in the model the anisotropy in the relative dielectric constant of ruby. Currently, we consider the dielectric constant to be slightly variable. Its value can be adjusted by varying the small air gap between the ruby and the top wall of the cavity that contains it.

We assume that the frequency-dependent part of the effective scalar susceptibility is contained totally within the line-shape functions. Strictly speaking, this is not true. As the frequency is changed, the field distribution within the ruby cavity will change slightly. This will lead to slightly different values for the susceptibility. As an example of this, we consider a coupled-cavity maser designed to amplify over 50 MHz centered at 8.425 GHz. A perspective view of this is shown in Fig. 3. If the quantity χ_p is evaluated inside the passband of the structure, a small variation with frequency can be seen. This is shown in Fig. 4 for five slices within the ruby-filled cavity. The slices are oriented perpendicular to the z-direction and are located at the two irises, the center of the cavity, and approximately 1/4 and 3/4 of the length of the cavity. The variation is essentially linear with frequency. Over the 8.40- to 8.45-GHz band, it is about 2 to 3 percent for the three slices nearest the coupling cavity and essentially independent of frequency over the last two slices. The behavior will depend on the particular microwave structure being evaluated and should be checked by the designer. In this case, the value of χ_p at 8.425 GHz represents the actual value for the frequencies of interest to within about ± 1 percent.

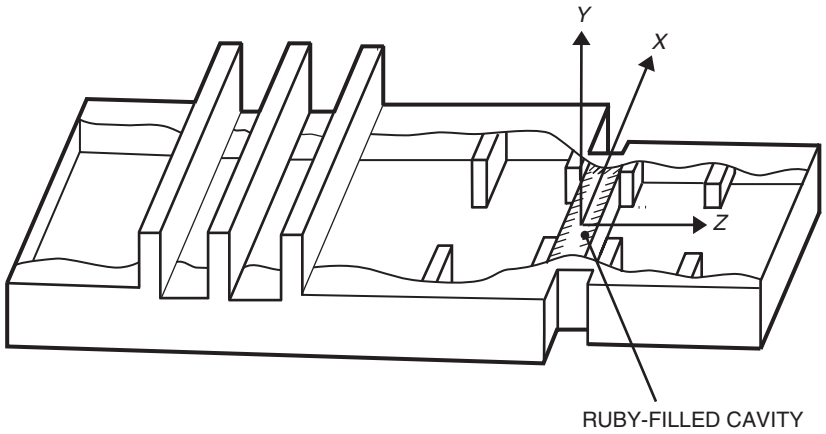

Fig. 3. A perspective view of a coupled-cavity maser. The cavities are drawn for illustrative purposes only; they are not to scale.

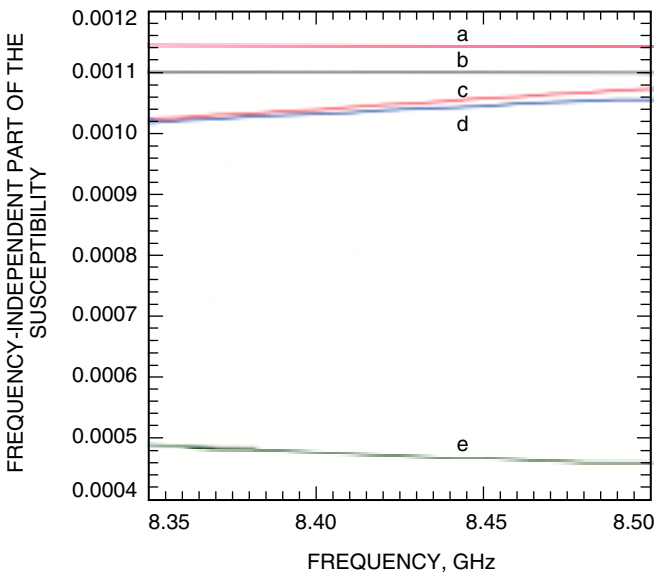

Fig. 4. The frequency variation of χ_p for five slices in the ruby-filled cavity. Curves "a" through "e" correspond to slices near the pump iris, 1/4 of the cavity length from the pump iris, near the signal iris, 1/4 of the cavity length from the signal iris, and at the center of the cavity, respectively.

Finally, the program does not address the question of ohmic losses in the copper. Experimentally, they are very small (especially at cryogenic temperatures) and are not considered a major factor in the prediction of the maser response. Nevertheless, it is a topic that may be included in future versions of the program.

Some comparisons of the model with data have already been made and are discussed in the next section. However, these are not particularly stringent tests of the model. It would be desirable to test the model more extensively in the future.

V. Examples

A. Ruby-Filled Waveguide at Room Temperature

We consider ruby absorption at 31.5 GHz at room temperature. The comparison with data from reflection-type cavities at cryogenic temperatures is often obscured by variation in the frequency-dependent loss or ripple due to unavoidable mismatches in the waveguide between the generator and the maser. These mismatches affect the coupling to the cavities. A transmission measurement of a well-matched ruby-filled waveguide is chosen to provide a better test of the program's ability to predict the strength of the maser action. The ruby-filled waveguide is well matched because the copper waveguide and the alumina input and output pieces are tapered. The structure used for this test is shown in Fig. 5(a). Since the program will not handle partially filled waveguide, a rectangular bar of ruby was placed in the center of the test structure with the alumina pieces serving only to provide a good match into and out of the ruby bar.

The length of the ruby bar is 5.969 cm. This length is too large to be totally within a homogeneous region of the small electromagnet used for the measurements. Therefore, the measured ruby absorption line shape is not Lorentzian, but approximately sawtooth shaped. The measured ruby spin resonance absorption is shown in Fig. 5(b).

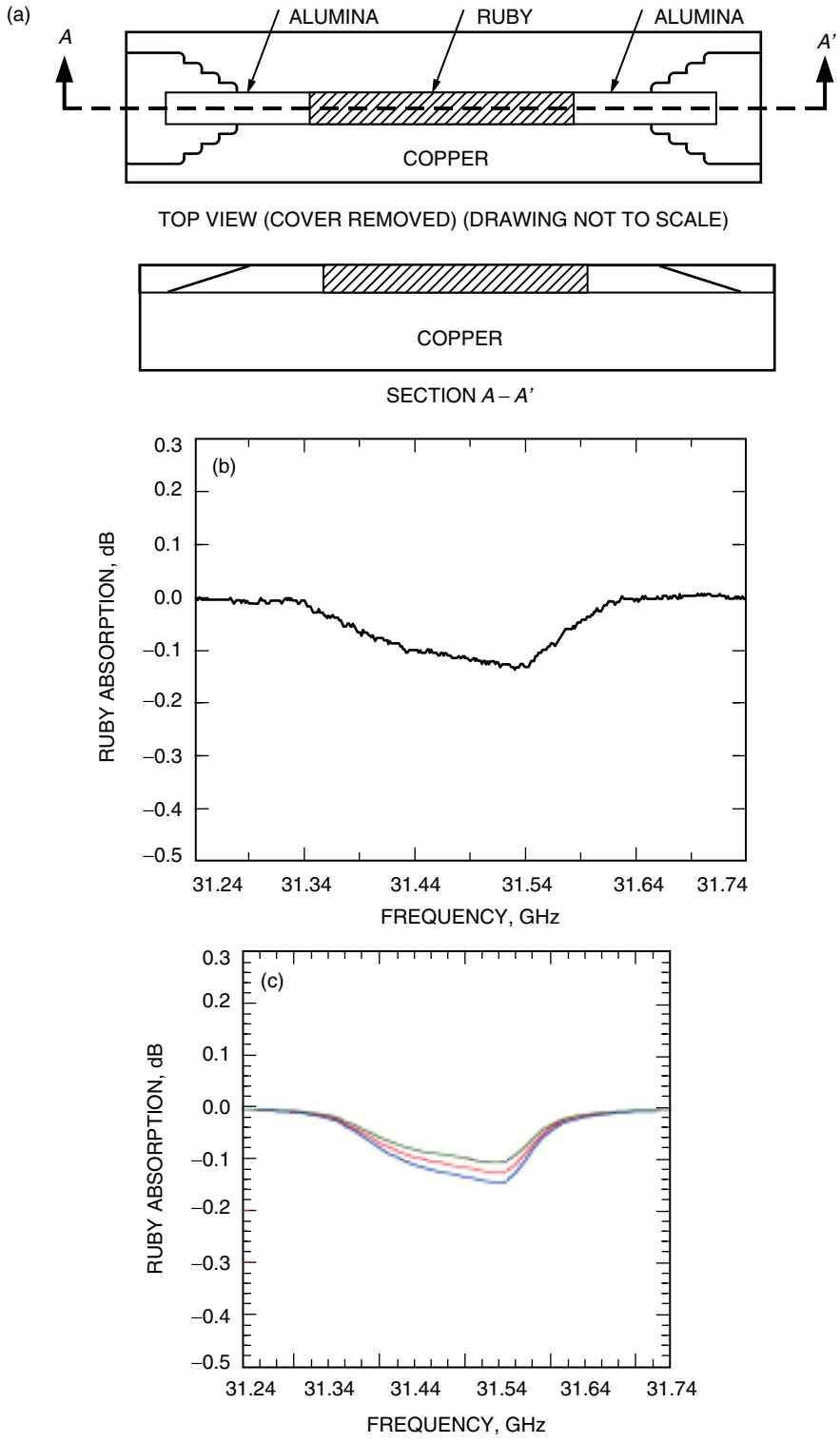

Fig. 5. Test structure, data, and theory for a well-matched ruby-filled waveguide in a nonuniform magnetic field: (a) microwave test structure used to obtain the data in Fig. 5(b), (b) measured power absorption due to the ruby spin resonance at room temperature, and (c) calculated power absorption using the spin system model for χ_p = 0.0000357, 0.0000420, and 0.0000483.

In order to model this situation, a magnetic field gradient along the length of the ruby bar must be simulated. The program does this by assigning different resonant frequencies to different sections of the ruby bar. The curves in Fig. 5(c) were made assuming 10 sections of ruby, each resonant at a slightly different frequency, with a total length of 5.969 cm. The line width of each section was 60 MHz, and the relative dielectric constant of the ruby was taken to be 9.5.

Once the shape was nearly fit, the value of χ_p was chosen to best fit the data. (Recall that χ_p includes everything except the line-shape functions.) In order to obtain the best fit to the data in Fig. 3(b), $\chi_p \approx 0.000042$. (This value includes an additional factor of 10^{-9} that actually belongs to the line-shape functions. However, the frequencies in the computer program (including the line width) are expressed in GHz rather than Hz. Since $g(f)$ and $h(f)$ have dimensions of frequency^{-1}, the line-shape values are too large by a factor of 10^9.) Also plotted are two curves where χ_p was increased and decreased by 15 percent. The relatively small changes indicate this is not a precision test of the model.

Nevertheless, we evaluate Eq. (15). The values used were $S_{eff} = 0.956$, $\mu_o = 4\pi \cdot 10^{-7}$ H/m, $\beta = 9.273{\cdot}10^{-24}$ A-m^2, $h = 6.626{\cdot}10^{-34}$ J-s, and $g_s = 2.0$. The above values imply $(n_3 - n_2) = 2.14 \times 10^{22}$ spins per cubic meter. This spin-population difference at 296 K implies a total spin density of 1.65×10^{25} spins per cubic meter. If the ruby is grown by mixing 0.05 percent by weight of Cr_2O_3 with Al_2O_3, then the total number of spins per cubic meter is 1.58×10^{25}. Thus, the nominal growth value and the value suggested by the data agree quite well.

Incidentally, even if the magnetic field were uniform, on resonance the line-shape function would be $g(f_o) = 2/\pi\Delta f_L = 2/\pi(0.060) = 10.61$. This quantity multiplied times 0.000042 equals 0.000446. This is the ac susceptibility on resonance. Even at cryogenic temperatures near 4.2 K, where the susceptibility is perhaps 70 times greater, the value is only 0.0312. It is seen that $\chi << 1$. This value of χ'' implies a magnetic Q of $Q_m = 1/\chi'' = 32$.

B. Ka-Band Multiple-Cavity Maser: Ruby Absorption and Mismatch Effects

We next consider the Ka-band multiple-cavity maser at 4.2 K. The measured data are shown in Fig. 6(a) and indicate a minimum return loss of nearly −35 dB. However, the spin system is nearly critically coupled at this temperature. Slight changes in the match can affect the measurement significantly. The calculated return loss is shown in Fig. 6(b) as the ruby resonance is tuned in frequency. To make this plot, we introduced a discontinuity in the waveguide about 38 cm in front of the maser. (This is the approximate location of a waveguide circulator in the experimental setup.) The return loss of the discontinuity was set to be about −23 dB. Then the ruby resonance was swept in frequency. This corresponds to tuning the applied static magnetic field. The absorption is very sensitive to the impedance seen by the maser. The return loss can vary from nearly −23 dB to about −13 dB. A better test of the program at cryogenic temperatures is possible if we move away from the center of the dielectric resonance. Then the spin system will not be nearly critically coupled and should be less susceptible to mismatches. This is considered next.

C. Ka-Band Multiple-Cavity Maser: Ruby Absorption and Reactive Effects

We consider the maser spin system tuned to the low-frequency side of the dielectric cavity resonance. In particular, the static magnetic field is adjusted until the spin resonance occurs at 31.377 GHz. The ruby spin absorption is much weaker and less susceptible to mismatch effects. We demonstrate the ability of the program to predict reactive effects by inverting the ruby spin system.

The reactance of the ruby resonance is dependent on χ'. Like χ'', it changes sign when the ruby spin population is inverted. Figure 7(a) shows the measured data. The lower curve is the ruby absorption. The maximum ruby absorption is 4 dB. The upper curve is the ruby inverted. In this particular case, the ruby absorption does not invert "straight up." The gain peak occurs about 20 MHz higher in frequency

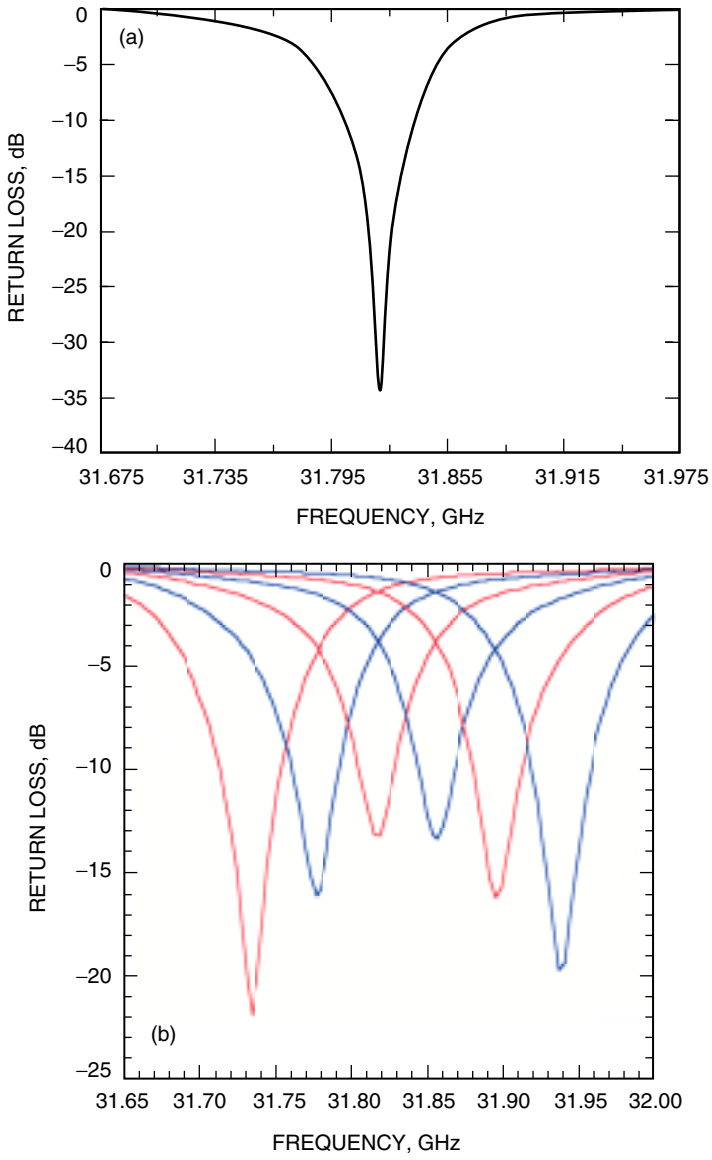

Fig. 6. Ka-band maser ruby absorption: (a) measured ruby absorption at a physical temperature near 4.2 K for the Ka-band multiple-cavity maser and (b) calculated ruby absorption as the external magnetic field is varied. A small mismatch has been placed 38 cm in front of the maser.

than the maximum absorption. If we were on the high-frequency side of the dielectric resonance, the gain peak would be lower in frequency than the maximum absorption. Figure 7(b) shows the results of the model. The physical temperature of the ruby in the data and the model was about 4.6 K. The predicted maximum ruby absorption is 5.1 dB, and the shift in frequency upon inverting the ruby is 28 MHz.

D. X-Band Multiple-Cavity Maser

The last example is an 8.40- to 8.45-GHz (X-band) coupled-cavity maser. It demonstrates the full utility of the model, which is not seen at Ka-band. The optimum signal polarization at Ka-band is nearly circular and, consequently, is essentially independent of position in the ruby-filled cavity. This is not the case at X-band. Consider the maser structure shown in Fig. 3. We will examine two cases, one with

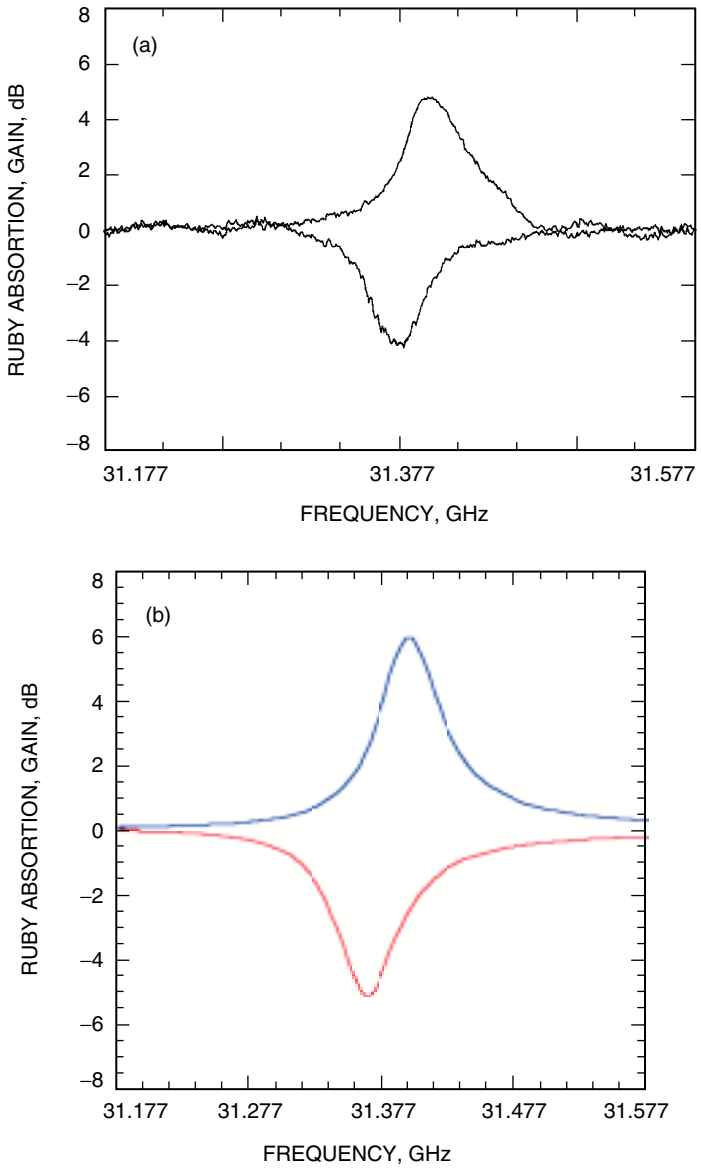

Fig. 7. Ka-band maser ruby absorption/gain: (a) measured ruby gain and absorption for the Ka-band multiple-cavity maser at a physical temperature of approximately 4.6 K; the frequency of the measurement is well below the center frequency (approximately 32 GHz) of the dielectric resonance, and (b) calculated ruby gain and absorption for the conditions of Fig. 7(a).

the ruby c-axis oriented in the x-direction and the other with the c-axis in the z-direction. The cavity that holds the ruby is 2.291 cm by 0.6528 cm in the x- and z-directions, respectively. (The greater the deviation from a square cavity, the greater will be the effect of changing the ruby c-axis orientation.) The coupled-cavity bandwidth is approximately 100 MHz, and the ruby line width is given a linear taper of about 60 MHz. The magnetic field taper imposed on the ruby is along the direction of propagation. The ruby cavity is broken up into 21 equal slices. The magnetic field version of the mode-matching program is run to determine the effective susceptibility in each slice. The program creates a file suitable for use by the s-parameter mode-matching program. The predicted ruby absorption for the two cases is shown in Fig. 8 for the cavity at 4.0 K.

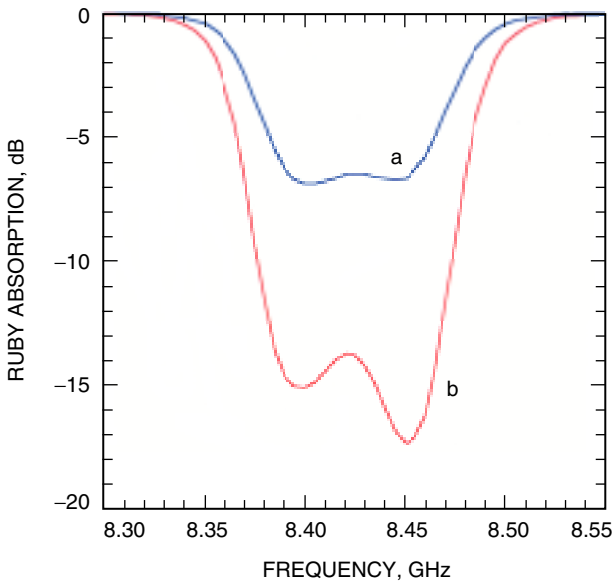

Fig. 8. Calculated ruby absorption for an X-band coupled-cavity maser showing the effects of c-axis orientation. Curve "a" corresponds to the ruby c-axis oriented in the z-direction. Curve "b" corresponds to the ruby c-axis oriented in the x-direction.

VI. Conclusion

The mode-matching program used to design masers has been improved to allow modeling of the ruby spin system. It is shown how this can be done using a frequency-dependent complex scalar magnetic susceptibility. It is shown how the value of this parameter can be evaluated knowing the physical properties of ruby, the geometry of the cavities, and the physical operating conditions. The program allows for the ruby to be in either the absorbing or emitting state. Several examples demonstrating the program are presented.

Acknowledgments

The author would like to thank Bob Clauss for many useful discussions. He also suggested using the broadened data in Fig. 5 and provided the X-band maser input file used for Fig. 8. Thanks also to Dr. Dan Hoppe for useful discussions regarding the propagation constant.

References

[1] D. J. Hoppe, "Modal Analysis Applied to Circular, Rectangular, and Coaxial Waveguides," *The Telecommunications and Data Acquisition Progress Report 42-95, July–September 1988*, Jet Propulsion Laboratory, Pasadena, California, pp. 89–96, November 15, 1988.
http://tmo.jpl.nasa.gov/tmo/progress_report/42-95/95I.PDF

[2] J. S. Shell and R. C. Clauss, "A 32-Gigahertz Coupled-Cavity Maser Design," *The Telecommunications and Mission Operations Progress Report 42-142, April–June 2000*, Jet Propulsion Laboratory, Pasadena, California, pp. 1–22, August 15, 2000.
http://tmo.jpl.nasa.gov/tmo/progress_report/42-142/142G.pdf

[3] J. Shell, "Radio Frequency Fields in Multiple-Cavity Masers," *The InterPlanetary Network Progress Report 42-146, April–June 2001*, Jet Propulsion Laboratory, Pasadena, California, pp. 1–14, August 15, 2001.
http://tmo.jpl.nasa.gov/tmo/progress_report/42-146/146H.pdf

[4] A. E. Siegman, *Microwave Solid State Masers*, New York: McGraw-Hill Book Company, 1964.

[5] H. Kiemle, "Die Komplexe Magnetische Suszeptibilitat von Rubin fur Microwellen-Maser," *Zeitschrift fur Angewandte Physik,* vol. 18, pp. 260–264, 1964.

[6] J. Shell, "The Paramagnetic Ground State of Ruby—Revisited", *The Interplanetary Network Progress Report 42-150, April–June 2002*, Jet Propulsion Laboratory, Pasadena, California, pp. 1–14, August 15, 2002.
http://ipnpr.jpl.nasa.gov/progress_report/42-150/150K.pdf

[7] B. Lax and K. J. Button, *Microwave Ferrites and Ferrimagnetics,* New York: McGraw-Hill Book Company, 1962.

Appendix

Derivation of an Effective Scalar Susceptibility

A derivation of an effective scalar susceptibility is discussed by Siegman and Lax and Button [4,7]. We briefly discuss it here.

In general, the change in the propagation constant due to magnetic tensor loading is given by

$$\gamma + \gamma_o^* = \frac{j\omega \iint \overrightarrow{H} \cdot \overline{\overline{\Delta\mu}} \cdot \overrightarrow{H_o^*} dS}{\iint \overrightarrow{z} \cdot (\overrightarrow{E} \times \overrightarrow{H_o^*} + \overrightarrow{E_o^*} \times \overrightarrow{H}) dS} \tag{A-1}$$

where γ, γ_o are the perturbed and unperturbed propagation constants and $\overline{\overline{\Delta\mu}}$ is the change in the permeability tensor due to the magnetic loading. Also, $\overrightarrow{E_o}, \overrightarrow{H_o}$ are the unperturbed electric and magnetic fields, and $\overrightarrow{E}, \overrightarrow{H}$ are the fields in the presence of the spin system. The first approximation is to replace the perturbed fields by the unperturbed fields. Then the denominator in Eq. (A-1) is four times the power flow down the waveguide in the absence of the spin system. But the power flow is the group velocity times the stored energy integrated over the waveguide cross-section. In particular,

$$P = v_g W_s = v_g \left(\frac{1}{2} \mu_o \iint \overrightarrow{H_o^*} \cdot \overrightarrow{H_o} dS \right) \tag{A-2}$$

Since $\overline{\overline{\Delta\mu}} = \mu_o \overline{\overline{\chi}}$, we can write

$$\gamma + \gamma_o^* = \frac{j\omega \iint \overrightarrow{H_o^*} \cdot \overline{\overline{\chi}} \cdot \overrightarrow{H_o} dS}{2 v_g \iint \overrightarrow{H_o^*} \cdot \overrightarrow{H_o} dS} \tag{A-3}$$

Using a Taylor series expansion, Siegman shows that if a scalar magnetic susceptibility is present, the first-order changes in the real and imaginary parts of the propagation constant are given by

$$\Delta\beta - j\alpha = \frac{\omega}{2 v_g} (\chi' - j\chi'') \tag{A-4}$$

Comparison of Eq. (A-3), where $\gamma = \alpha + j\beta$ and $\gamma_o = j\beta_o$, and Eq. (A-4) leads to the effective susceptibility, Eq. (9), in the text.